AGU PUBLICATIONS

JGR

Journal of Geophysical Research: Space Physics

RESEARCH ARTICLE
10.1002/2016JA023718

Multi-instrument observation of simultaneous polar cap auroras on open and closed magnetic field lines

J. A. Reidy[1,2], R. C. Fear[1], D. K. Whiter[1], B. S. Lanchester[1], A. J. Kavanagh[2,3], L. J. Paxton[4], Y. Zhang[4], and M. Lester[5]

[1]Department of Physics and Astronomy, University of Southampton, Southampton, UK, [2]British Antarctic Survey, National Research Council, Cambridge, UK, [3]Rutherford Appleton Laboratory, Science and Technology Facilities Council, Didcot, UK, [4]The Johns Hopkins University Applied Physics Laboratory, Laurel, Maryland, USA, [5]Department of Physics and Astronomy, University of Leicester, Leicester, UK

Key Points:
- Evidence for two different mechanisms producing aurora in the polar cap occurring simultaneously
- Example of a polar cap arc formed on closed field lines
- Example of a polar cap arc formed on open field lines, embedded within polar rain

Supporting Information:
- Supporting Information S1
- Movie S1
- Movie S2

Correspondence to:
J. A. Reidy,
jr10g11@soton.ac.uk

Citation:
Reidy, J. A., R. C. Fear, D. K. Whiter, B. S. Lanchester, A. J. Kavanagh, L. J. Paxton, Y. Zhang, and M. Lester (2017), Multi-instrument observation of simultaneous polar cap auroras on open and closed magnetic field lines, *J. Geophys. Res. Space Physics*, *122*, 4367–4386, doi:10.1002/2016JA023718.

Received 22 NOV 2016
Accepted 23 FEB 2017
Accepted article online 11 MAR 2017
Published online 28 APR 2017

Abstract This paper presents observations of polar cap auroral features on 19 January 2008, evaluated using multiple instruments with near-simultaneous observations in both hemispheres. Analysis of the features indicates that there are at least two formation mechanisms/types of polar cap aurora occurring simultaneously on different magnetic field topologies (one on open and the other on closed magnetospheric field lines). Two high-latitude structures were observed on opposing sides of the northern hemisphere polar cap in the same time interval. The structure on the duskside was formed on closed field lines that protruded into the polar cap and was generated by the precipitation of electrons with energies varying between 2 and 11 keV consistent with an identified mechanism for the formation of transpolar arcs. However, the structure did not extend fully across to the dayside of the auroral oval but rather stayed at ~80° magnetic latitude for a minimum duration of 40 min. Thus, this structure is an example of a "failed" transpolar arc. The structure on the dawnside of the polar cap was associated with low-energy electron precipitation (less than 1 keV) and no associated ion signatures, which is consistent with it being a common low-intensity arc formed by accelerated polar rain on open field lines. The two separate types of polar cap auroras formed during the same interval, demonstrating the complexity of the solar wind-magnetosphere coupling during the interval.

1. Introduction

Polar cap auroras occur at high latitudes above the main auroral oval and are sometimes known as high-latitude or Sun-aligned arcs. These arcs have been studied for a century [*Mawson*, 1916] and are correlated with periods of quiet magnetospheric activity [*Davis*, 1963] and a northward directed interplanetary magnetic field (IMF) [*Berkey et al.*, 1976; *Gussenhoven*, 1982]. Their location in the polar cap and their motion are dependent on the IMF B_y component [*Frank et al.*, 1985; *Huang et al.*, 1989; *Craven et al.*, 1991; *Valladares et al.*, 1994; *Kullen et al.*, 2002]; however, there are exceptions to this dependence [e.g., *Hosokawa et al.*, 2011]. Whether these high-latitude auroras occur on the open field lines that define the region of the polar cap, or closed field lines embedded within the polar cap, is an open question. In a review, *Zhu et al.* [1997] suggested three different magnetospheric configurations that could result in the formation of high-latitude aurora. These configurations, along with multiple mechanisms that have been advocated for them are discussed below.

The first magnetospheric configuration is magnetotail lobe bifurcation whereby the closed field lines of the plasma sheet protrude into the magnetotail lobes. This idea was proposed after satellite UV images revealed large-scale Sun-aligned arcs emerging from the nightside oval, known as transpolar arcs or, when considering the entire configuration including the oval, "theta" aurora [*Frank et al.*, 1982, 1986]. *Frank et al.* [1982] also reported simultaneous plasma measurements from a low-altitude spacecraft that crossed the morning sector of the oval, a Sun-aligned arc, and then the evening oval. These measurements showed the electron spectra over the arc to be similar to those over the oval and hence led them to suggest that the arc was formed on closed field lines. Furthermore, polar rain, which originates from the solar wind, has been observed on either side of a Sun-aligned arc [*Hoffman et al.*, 1985]. This suggested that the arc was surrounded by open field lines, validating the idea of a bifurcated lobe.

Milan et al. [2005] proposed a mechanism explaining this magnetospheric configuration. Their mechanism is based on the nightside closure of open magnetotail flux during northward IMF, when dayside reconnection is suppressed and a twist in the magnetotail due to an IMF B_y component. The IMF B_y component is introduced some hours before during an earlier period of dayside reconnection and results in the northern and southern hemispheric lobes twisting about the GSE X axis [e.g., *Browett et al.*, 2016; *Tenfjord et al.*, 2015; *Reistad et al.*, 2016]. If reconnection occurs during these conditions, the return flow of the newly closed flux will be asymmetric about magnetic midnight [*Grocott et al.*, 2003, 2007], referred to by *Milan et al.* [2005] as TRINNIs ("Tail reconnection during IMF-northward, nonsubstorm intervals"). *Milan et al.* [2005] suggested that when a field line that straddles midnight is closed, it will become stuck due to equal and opposite forces being applied to either end of the field line as it tries to return to the dayside. As more and more flux is closed in this magnetic local time (MLT) sector, the trapped field lines will protrude deeper into the magnetotail lobes. This mechanism has been validated by several different case studies [e.g., *Goudarzi et al.*, 2008; *Fear et al.*, 2014]. Furthermore, the main predictions from the mechanism, i.e., a delay in the MLT dependence on the IMF B_y and an association with TRINNI flows, have been statistically verified by *Fear and Milan* [2012a, 2012b]. *Fear et al.* [2015] have also recently argued that this mechanism implies that the presence of a transpolar arc modifies the large-scale magnetospheric dynamics when high-latitude magnetopause (lobe) reconnection also takes place, as the lobe reconnection process is then capable of causing a net opening of magnetic flux.

Additionally, the *Milan et al.* [2005] mechanism predicts that transpolar arcs will form on opposite sides of the polar cap, determined by IMF B_y component, in opposite hemispheres. In fact, any mechanism which place transpolar arcs on closed field lines, predicts that they will be seen in both hemispheres simultaneously. Conversely, *Østgaard et al.* [2003] presented two intervals with simultaneous northern and southern auroral observations, where a transpolar arc was only seen in one hemisphere. *Fear and Milan* [2012a] suggested that these observations could still be explained by the *Milan et al.* [2005] mechanism if reconnection occurred preferentially in the summer hemisphere [*Crooker and Rich*, 1993; *Lavraud et al.*, 2005], and hence, the transpolar arc in the summer hemisphere moved and became indistinguishable from the main oval before the first available image from that hemisphere. However, further study of so-called "nonconjugate" transpolar arcs is warranted.

The second magnetospheric configuration that *Zhu et al.* [1997] outlined was related to oval expansion. *Meng* [1981] suggested that after a period of southward IMF, the edge of the auroral oval could expand poleward resulting in aurora seen at higher latitudes, essentially identifying regular auroral features observed in the main oval as polar cap arcs. This idea was based on observations of continuous soft (<1 keV) electron precipitation from the main auroral oval up to high latitudes (>80°) and simultaneous observations of Sun-aligned arcs in the polar cap. They suggested that the arcs were occurring on closed field lines at the expanded poleward edge of the oval rather than on the open field lines of the polar cap.

The final configuration *Zhu et al.* [1997] discussed was where polar cap arcs form on open field lines. There have been studies reporting Sun-aligned arcs embedded within polar rain [e.g., *Hardy et al.*, 1982]. A study by *Carlson and Cowley* [2005] found subvisual Sun-aligned arcs to be consistent with accelerated polar rain and suggested that they can be generated by any method that drives shear flows across open field lines. These subvisual, lower intensity arcs are thought to dominate the polar cap during northward IMF and are reported to be present in the polar cap at least 40% of the time [*Valladares et al.*, 1994], whereas the larger, transpolar arcs are present approximately only 10% of the time [*Kullen et al.*, 2002]. This is reflected in the 130 transpolar arcs identified over a 5 year interval in a statistical survey of global-scale images carried out by *Fear and Milan* [2012a], compared to the 150 Sun-aligned arcs identified in *Valladares et al.* [1994] using ground-based all-sky cameras from Qannaaq, Greenland, in just one winter season.

Some authors have suggested that multiple mechanisms may be required to explain the discrepancy in the observations of polar cap auroras. A statistical study by *Kullen et al.* [2002] classified five different types of transpolar arcs depending on their motion, structure, and where they formed within the polar cap. The authors, at the time, could not find a mechanism that explained more than one of these types and hence concluded there must be at least five different formation mechanisms. However, in *Kullen et al.* [2015], the same transpolar arcs were re-evaluated using data from the Super Dual Auroral Radar Network (SuperDARN), and TRINNI flows were found for three out of the five types, confirming the validity of the predictions made by *Milan et al.* [2005] and consistent with the observations of *Fear and Milan* [2012a, 2012b]. One type that did not show these flows were the arcs classified as "bending arcs"; these arcs have since been identified as a phenomenon

of dayside reconnection under IMF B_y-dominant conditions [*Carter et al.*, 2015]. Conversely, it has been argued that some transpolar arcs are formed by a more complicated process whereby two different mechanisms, one on the dayside and the other on the nightside, occur simultaneously [*Eriksson et al.*, 2005; *Mailyan et al.*, 2015].

Separately, in a ground-based statistical study, *Hosokawa et al.* [2011] argued that the motion of only some arcs was correlated with the sign of IMF B_y, while others moved independently from it. They suggested that the motion of the B_y-dependent arcs is caused by flux transfer due to lobe reconnection, indicating that the plasma source for these arcs is on or adjacent to open field lines. As the B_y-dependent arcs are seemingly unaffected by lobe reconnection, *Hosokawa et al.* [2011] suggest that they are formed on closed field lines, indicating a different formation mechanism for each type. However, another possible explanation for the apparent difference between "B_y-dependent" and "B_y-independent" polar cap arc motion could be that the motion is driven by polar cap convection as outlined by *Milan et al.* [2005], which would result in the same spatial patterns as reported by *Hosokawa et al.* [2011].

In a review of polar precipitation and aurora, *Newell et al.* [2009] argued for three types of polar cap aurora: the first, a common but weak arc caused by an intensification of polar rain (no associated ion precipitation); the second, arcs seen adjacent to the auroral oval associated with higher electron flux and an ion signature; lastly, a rare high-energy type consistent with transpolar arcs.

The aim of this study is to combine ground-based and satellite observations of polar cap auroras to investigate the suggestion that some polar cap arcs form on open field lines, while others form on closed field lines and to investigate whether it is possible for both configurations to form at the same time. This study considers any high-latitude aurora that is distinctly Sun-aligned in nature and shown to originate from either accelerated polar rain or a protrusion of the plasma sheet into the magnetotail lobes to be polar cap aurora [*Newell et al.*, 2009]. We present observations from satellites and several ground-based instruments from 19 January 2008. An introduction to the instruments used in this study is presented in section 2, followed by the main findings and observations in section 3. Finally, in section 4 these observations are discussed and conclusions are drawn on the configuration of the magnetosphere during northward IMF conditions.

2. Instrumentation

Measurements from multiple instruments were used to analyze the magnetospheric and ionospheric conditions during the event studied. In addition to the main instruments that are discussed in the following three subsections, we make use of data from the fluxgate magnetometer (FGM) instruments [*Balogh et al.*, 2001; *Gloag et al.*, 2010] and the Hot Ion Analyzer on the Cluster Ion Spectrometry instrument (CIS-HIA) [*Rème et al.*, 2001; *Dandouras et al.*, 2010] on the Cluster 3 spacecraft for the solar wind conditions. Magnetometer data from the International Monitor for Auroral Geomagnetic Effects (IMAGE) Svalbard stations were also obtained [*Tanskanen*, 2009].

2.1. The Special Sensor Ultraviolet Spectrographic Imager

The Special Sensor Ultraviolet Spectrographic Imager (SSUSI) instruments are on board four of the DMSP (Defense Meteorological Satellite Program) spacecraft [*Paxton et al.*, 2002]. The SSUSI imagers on two of the DMSP spacecraft (F16 and F17) were operational during our event. The DMSP satellites are in a Sun-synchronous orbit with a period of approximately 90 min. SSUSI scans from horizon to horizon above the polar region in each hemisphere, building up brush-stroke-like images of the aurora. A scan of the polar auroral region takes approximately 20 min.

SSUSI produces these images in five different UV wavelengths simultaneously. In this study the Lyman-Birge Hopfield long (LBHL) band, between 165 and 180 nm, is used. For comparison with observations of polar cap aurora by the IMAGE satellite [e.g., *Milan et al.*, 2005; *Fear and Milan*, 2012a, 2012b; *Fear et al.*, 2014, 2015], these wavelengths are within the range of the IMAGE wideband imaging (WIC) camera.

2.2. The EISCAT Svalbard Radar

The EISCAT (European Incoherent Scatter) Svalbard radar (ESR) is an incoherent scatter radar situated at Longyearbyen in the Svalbard archipelago. It is operated by the European Incoherent Scatter Scientific Association. The ESR consists of a steerable 32 m diameter dish antenna and a colocated 42 m fixed dish antenna that is aligned with the local magnetic zenith [*Wannberg et al.*, 1997]. During the international Polar Year (IPY) between 2008 and 2009, when our event occurred, the ESR operated quasi-continuously taking

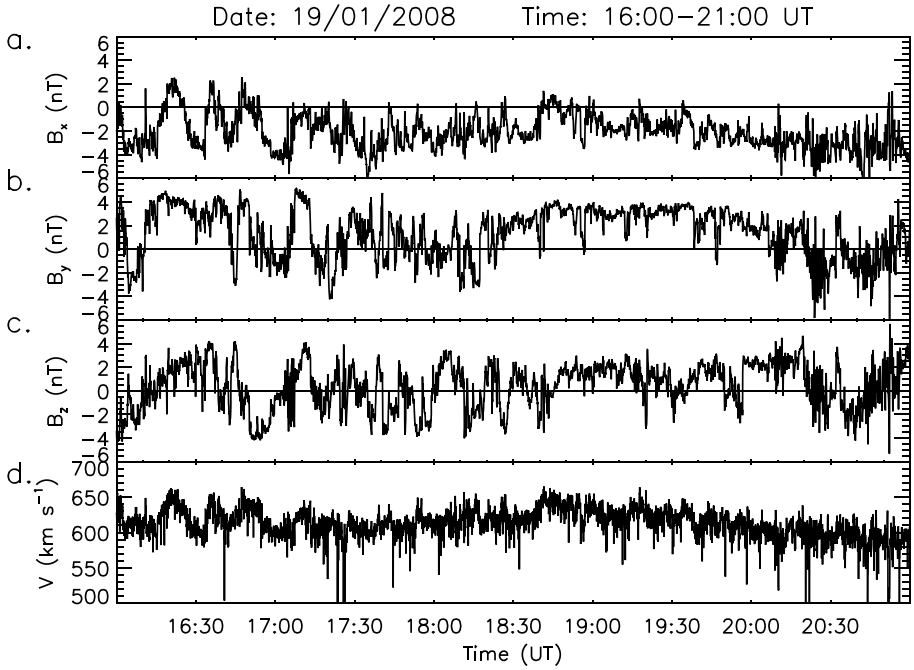

Figure 1. IMF data from the Cluster spacecraft between 16:00 and 21:00 UT. The top three panels are the IMF GSM components (a) B_x, (b) B_y, and (c) B_z at spin resolution. (d) The solar wind speed.

measurements of ionospheric parameters (electron density and temperature and ion temperature with the 42 m dish at a 6 s resolution). In this study, data from the ESR, during the IPY, have been analyzed for our period of interest, and electron density profiles have been used to estimate the energy of precipitation using the Southampton ionospheric model [*Lanchester et al.*, 1998] (described in section 2.4).

2.3. The Auroral Structure and Kinetics Instrument

The ASK (Auroral Structure and Kinetics) instrument is a multispectral, high-resolution auroral imager [*Ashrafi*, 2007; *Dahlgren et al.*, 2008] located at the ESR site. The imager consists of three cameras (ASK1, ASK2, and ASK3), each observing the same narrow field of view of 3.1° × 3.1°, equivalent to 5 × 5 km at a height of 100 km, in the magnetic zenith. Each camera has a different narrow passband interference filter to select specific auroral emissions. In this study, images from the ASK1 and ASK3 cameras obtained at 20 frames per second are used. These camera images correspond to the N_2 1PG (1st positive) emission at 673.0 nm and OI ($3s^5S$-$3p^5P$) emission at 777.4 nm.

The ASK instrument has been used to study auroral features at small spatial scale, for example, boundary undulations or "ruffs" [*Dahlgren et al.*, 2010] and at high temporal resolution to study flickering aurora [*Whiter et al.*, 2010]. The two main strengths of ASK are the ability to estimate the energy of precipitation and to trace plasma flows, which can in turn be used to estimate electric field strength and direction to very good resolution; these methods are outlined in a review paper by *Dahlgren et al.* [2016].

2.4. The Southampton Ionospheric Model

The Southampton ionospheric model (described in the appendix of *Lanchester et al.* [2001]) is a combined electron transport and ion chemistry model. The electron transport part [*Lummerzheim*, 1987] allows for an arbitrary input electron precipitation spectrum, provides ion production rates, and allows calculation of selected prompt optical emission rates. The ion chemistry part solves the coupled continuity equations for major and some minor ion species time dependently. The model assumes a neutral atmosphere taken from MSIS E-90 thermospheric model [*Hedin*, 1991] and requires input solar activity parameters for the date of event.

Data from ASK can be used in conjunction with the Southampton ionospheric model using a method outlined in *Lanchester et al.* [2009] to estimate the energy of the precipitating electrons. This method compares the ratio of emissions measured by the ASK1 and ASK3 cameras to a modeled relation between the ratio and energy produced by the ionospheric model. The ASK1 camera has a filter that is sensitive to high-energy

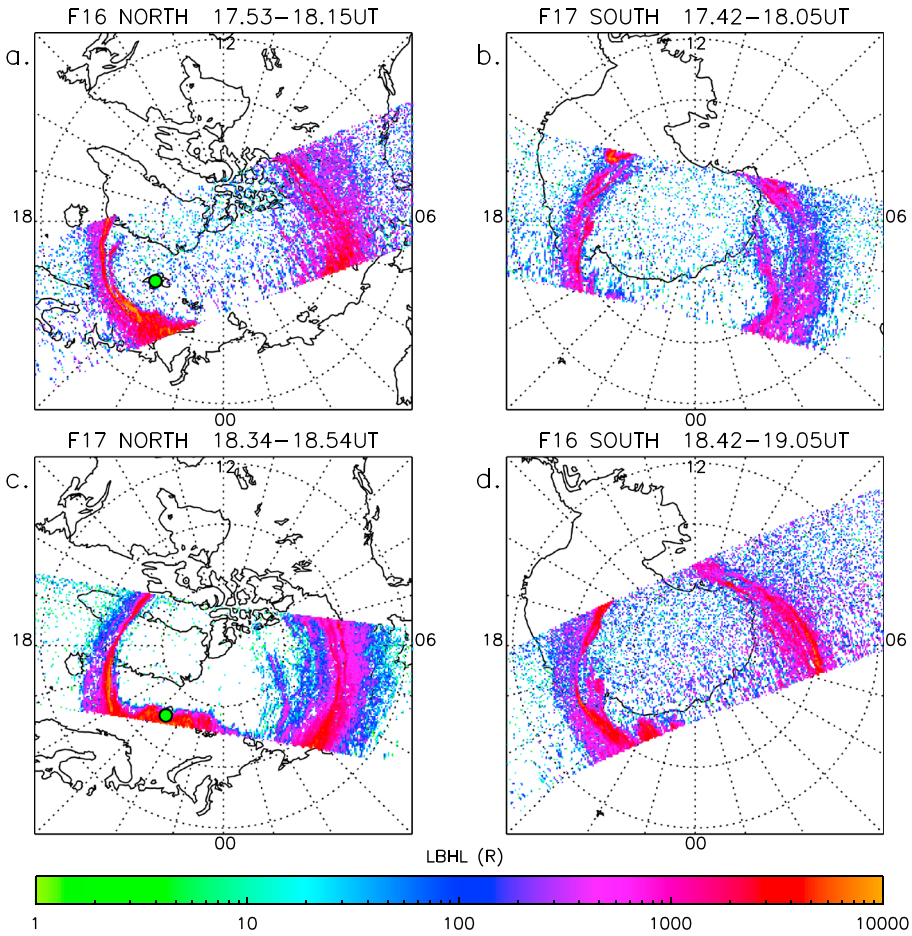

Figure 2. Images from SSUSI (LBHL band) between 17:50 and 19:05 UT providing almost simultaneous measurements of the Northern and Southern Hemispheres with two DMSP spacecraft, F16 and F17. (a, c) The Northern Hemisphere images are shown in the left hand column and (b, d) the southern in the right hand column. The southern hemisphere images have been reversed about the noon midnight meridian for ease of comparison. In all images noon is at the top and dawn to the right. The green dot in the Northern Hemisphere images indicates the position of ASK/ESR on Svalbard.

electron precipitation. ASK3 is sensitive to lower energy precipitation and hence the ratio of ASK3/ASK1 can provide characteristics of the energy of the precipitating electrons.

The ionospheric model can also be used to fit ionization rates inferred from ESR electron density profiles to estimate the energy of auroral precipitation *Lanchester et al.* [1998]. More details of this method is given in section 3.2.2.

2.5. Super Dual Auroral Radar Network

Super Dual Auroral Radar Network (SuperDARN) is a network of high-frequency coherent scatter radars that measure ionospheric flows in the polar regions of the Northern and Southern Hemispheres [*Greenwald et al.*, 1995; *Chisham et al.*, 2007]. This study uses data from the Pykvibaer radar, which has a field of view over Svalbard. During this period, it was operating in stereo mode, i.e., operating quasi-simultaneously on two different frequencies allowing for different spatial and temporal resolutions [*Lester et al.*, 2004]. We also use summarized global-scale data from the map-potential technique [*Ruohoniemi and Baker*, 1998] in which data from all radars are combined with data from a statistical model to obtain ionospheric flow patterns in the high-latitude regions.

3. Results

3.1. Interplanetary Conditions and Large-Scale Auroral Observations

We present a case study of high-latitude aurora on 19 January 2008. Figure 1 shows the solar wind conditions between 16:00 and 21:00 UT on this day provided by the Cluster 3 spacecraft. Figures 1a–1c show the IMF

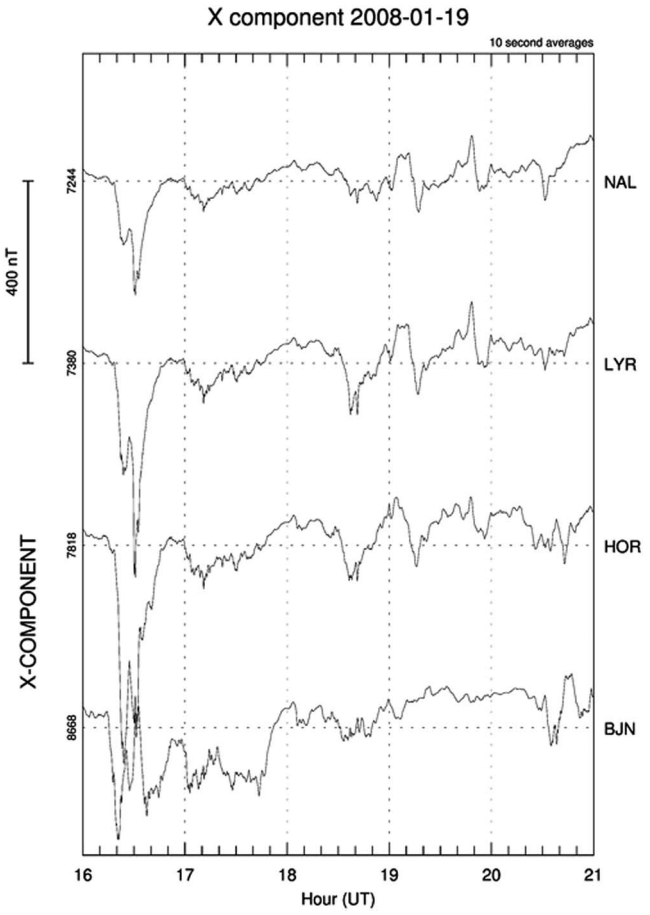

Figure 3. Magnetic field deflections in the *X* component (north) obtained from the IMAGE magnetometer Svalbard stations between 16:00 and 21:00 UT.

components in the Geocentric Solar Magnetospheric (GSM) coordinate system, Figure 1d shows the solar wind speed. The ion and electron spectrograms (not shown) confirm that Cluster was in the solar wind during our event, just upstream from the bow shock, at (14, 12, −8) R_E. Our period of interest is between 18:00 and 21:00 UT. During this time the IMF B_y component was predominately positive with the occasional negative turn. The IMF turned northward at around 18:45 UT and apart from a few brief southward turns, remained so until around 20:30 UT. Prior to this the IMF alternated between northward and southward. The B_x component was predominately negative throughout the interval. It can be seen in Figure 1d that this is a period of high solar wind speed with a mean value of 610 km s^{-1}.

Figure 2 show images from the SSUSI instruments on board DMSP F16 and F17 from 17:50 to 19:05 UT. During this interval the spacecraft provide almost simultaneous measurements of the Northern and Southern Hemispheres. Each image has been projected onto an MLT grid with noon at the top and dawn to the right. All of the Southern Hemisphere images have been reversed about the noon-midnight meridian for ease of comparison, such that dawn is to the right in all figures. Consequently, the spacecraft are traveling in the opposite direction in each hemisphere, i.e., left to right in the Northern Hemisphere image and vice versa in the southern image.

Figures 2a and 2b show images of the Northern Hemisphere between 17:53 and 18:15 UT and the Southern Hemisphere between 17:42 and 18:05 UT, respectively. These images coincide with the period when the IMF was alternating between northward and southward. The green dot in the Northern Hemisphere images indicates the position of ASK/ESR on Svalbard, which at this time are situated poleward of the auroral oval and are within the polar cap, looking along open field lines. The Southern Hemisphere image shows a Sun-aligned structure on the dawnside of the polar cap. This structure is not seen in any of the following images and is hence not considered a part of this study. The Northern Hemisphere between 18:34 and 18:54 UT and the

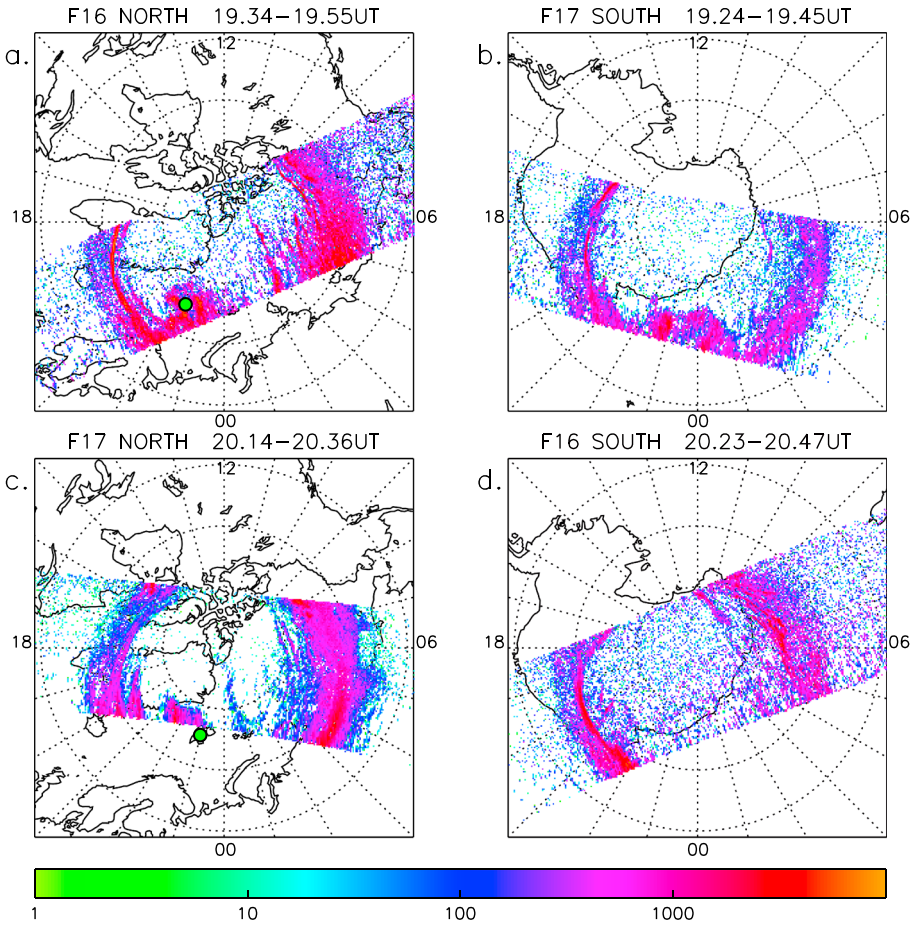

Figure 4. SSUSI images between 19:25 and 20:50 UT. Same layout as Figure 2 with noon at the top and dawn to the right; the Southern Hemisphere images have been flipped for ease of comparison. Again the green dot in the Northern Hemisphere indicates the location of Svalbard.

Southern Hemisphere between 18:42 and 19:05 UT are shown in Figures 2c and 2d. These images show the auroral regions around the time the IMF turned northward at 18:45 UT. In both hemispheres there is an auroral bulge seen between 21 and 24 MLT. In the Northern Hemisphere (Figure 2c), an approximately Sun-aligned arc can also be seen in the dawnside of the polar cap. No obvious counterpart to this structure can be seen in the almost simultaneous Southern Hemisphere image (Figure 2d).

Figure 3 shows data from the Svalbard magnetometers between 16:00 and 21:00 UT. A deflection can be seen around 16:30 UT, which likely corresponds to a magnetospheric substorm during the period of southward IMF [e.g., *Lühr et al.*, 1998]. At approximately 18:30 UT smaller deflections are seen, with the weakest deflections shown by the Bear Island magnetometer (BJN) and the strongest at Longyearbyen (LYR). This suggests that the activity may be localized to Svalbard, which is consistent with the bulges seen in the SSUSI image (Figure 2c). We hence suggest that the small, localized magnetic deflections are signatures of a poleward boundary intensification [*Lyons et al.*, 1999]. Hence, the bulges in the duskside of the Northern and Southern Hemispheres (Figures 2c and 2d) appear to result from flux closure in the tail, most likely at the far neutral line.

SSUSI observations between 19:24 and 20:47 UT are shown in Figure 4 with the same layout as Figure 2. Figures 4a and 4b correspond to the intervals between 19:34 and 19:55 UT for the Northern Hemisphere image and between 19:24 and 19:45 UT for the Southern Hemisphere. By this time the IMF had been generally northward for around an hour. The duskside bulge in the Northern Hemisphere (Figure 2c) has protruded further into the polar cap, extending over the field of view of ASK and ESR (green dot) to almost 80° magnetic latitude, becoming distinctly Sun-aligned in nature. A conjugate structure can still be seen in the Southern Hemisphere image, although this structure has not extended as far poleward. There are now also multiple Sun-aligned arcs seen in the dawnside of the Northern Hemisphere image, still with no apparent Southern

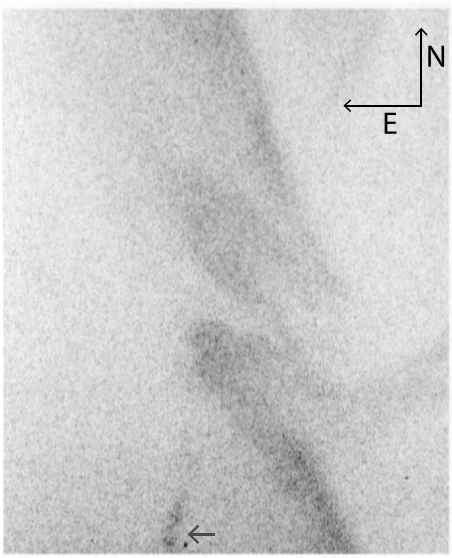

Figure 5. Image (in negative) obtained from a 60° field of view camera close to ASK at 20:23:23 UT. The camera is fitted with a 645 nm long pass filter. North is at the top and east is to the left as shown by the arrows. These directions are approximate as the camera is not sensitive enough to see stars, and hence, more accurate directions cannot be obtained. The arrow at the bottom of the image indicates moonlight.

Hemisphere counterpart. The last SSUSI images in our period of interest, between 20:14 and 20:36 UT in the Northern Hemisphere and between 20:23 and 20:47 UT in the Southern Hemisphere, are shown in Figures 4c and 4d, respectively. The duskside protrusion in the Northern Hemisphere over Svalbard remains after at least 45 min but has not grown further into the polar cap. The conjugate form is no longer seen in the Southern Hemisphere image, but this could be a result of the field of view of SSUSI. The Sun-aligned structure on the dawnside of the Northern Hemisphere image has now moved toward the noon-midnight meridian compared to the previous image.

3.2. The Duskside Structure

3.2.1. Analysis of Optical Data

Figure 5 shows an image of a north-south aligned arc over Svalbard taken by a 60° field of view camera from the Spectrographic Imaging facility (SIF), also located on Svalbard near the ESR/ASK site. Although this arc is not discernible in the SSUSI images, it forms part of the duskside structure observed in Figures 2c, 4a, and 4c. The arc entered SIF's field of view around 20:23:23 UT and moved eastward, i.e., dawnward. A video showing the 40 s interval when the arc passed through SIF's field of view is included in the supporting information.

Figure 6 shows observations from ASK taken during this selected interval (note that the 3° × 3° field of view of ASK is approximately in the center of the SIF image in Figure 5). Figure 6a shows the average intensity measured by ASK1, I_{6370} (black) and ASK3, I_{7774} (blue) in the 20 × 20 pixels surrounding the magnetic zenith between 20:23:25 and 20:23:40 UT. Snapshots were taken from the ASK1, I_{6370} camera in 1 s intervals between 20:23.29 and 20:23.36 UT, Figure 6c. The yellow box indicates the pixels averaged around magnetic zenith. The images show a bright curved structure sweeping through the ASK field of view from west to east, followed by a lower intensity more diffuse structure. The rapid changes in these images demonstrate the highly dynamic and small-scale structures within the larger-scale features.

The Southampton ionospheric model [*Lanchester et al.*, 2001] can be used to find the changes in energy flux and peak energy from the ratio of different wavelengths observed by the ASK instrument. The input to the model requires an initial shape for the spectrum of the incoming electrons, assumed to be a Gaussian in this study. Examples of the model production rates and emission height profiles for the emissions measured by ASK can be found in *Whiter et al.* [2010] and *Dahlgren et al.* [2011]. The height-integrated emissions are used to give a relationship between brightness ratio and peak energy, which is then compared with the measured brightness ratio to give the peak energy as plotted in Figure 6b. The energy flux is found from the brightness of the emission from N_2, which is almost independent of energy. A conversion factor of 240 R/(mW m^{-2}) obtained from the model is used to convert I_{6370} into flux.

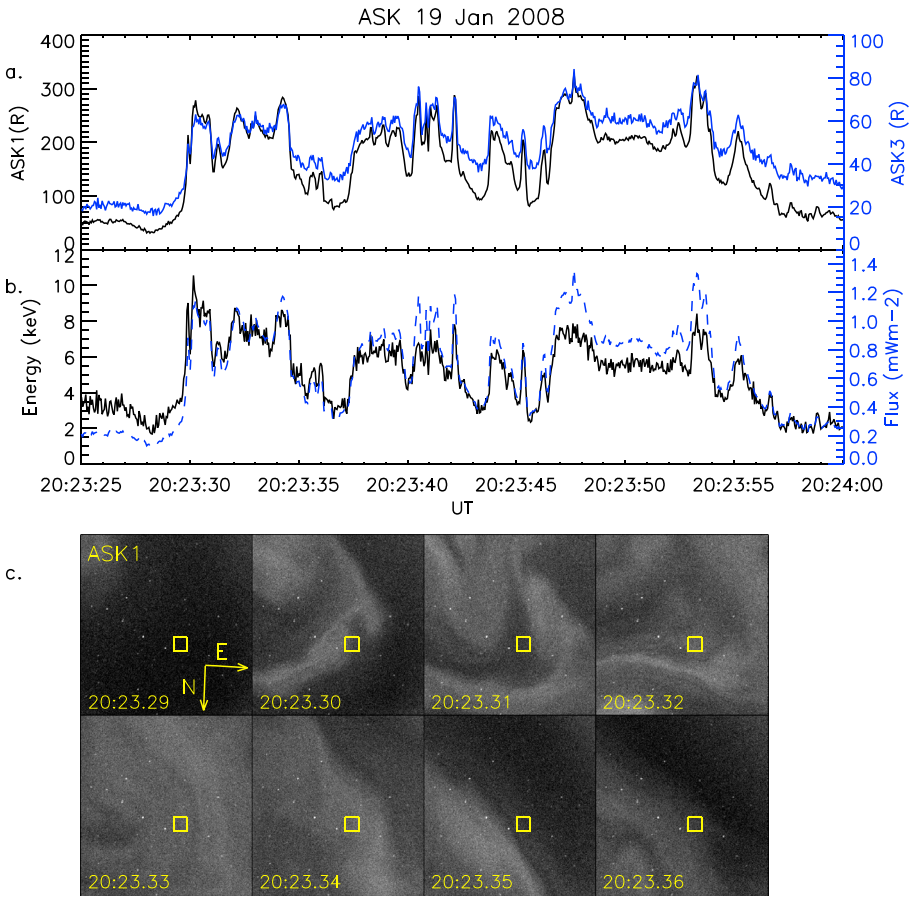

Figure 6. (a) The intensity from ASK1, I_{6370} (black) and ASK3, I_{7774} (blue) between 20:23.25 and 20:24.00 in the 20 × 20 pixels surrounding magnetic zenith. (b) The estimated energy (black) and energy flux (blue) of the precipitating electrons in the interval between 20:23.25 and 20:24.00 UT. (c) Snapshots from ASK1 between 20:23.29 and 20:23.36 UT in 1 s intervals. The yellow box in each image illustrates the pixels averaged around magnetic zenith. North is approximately at the bottom of the images and east is approximately left.

Figure 6b shows that the precipitation energy varies between 2 and 11 keV, with a mean value of 5 keV and a mean energy flux of 0.7 mW m^{-2}. This range also agrees with a similar study carried out by *Wu et al.* [1991] who observed a polar cap arc associated with precipitation energies between 3 and 12 keV. A video showing how the changes in energy correspond to ASK1 images over the selected interval is provided in the supporting information.

3.2.2. Analysis of ESR Height Profiles

Figure 7 shows the electron density (N_e), the electron temperature (T_e), and the ion temperature (T_i) profiles measured by the ESR between 17:00 and 22:00 UT, plotted at 1 min resolution. It can be seen that prior to 18:36 UT there is a cool *F* region plasma (above 200 km); after this time there is a sudden increase in the *E* region N_e down to heights of around 90 km with a corresponding increase in T_e (Figure 7b). These increases occur before the northward turning of the IMF at 18:45 UT and coincide with the start of the interval that SSUSI shows an auroral structure over Svalbard. They are typical signatures of precipitation on closed field lines. Furthermore, the T_e profiles show very cold plasma before 18:36 UT that is consistent with polar cap electrons. From this dramatic change in T_e, we suggest that the open/closed field line boundary has moved over the field of view of ESR (the open/closed field line boundary has previously been identified using T_e [e.g., *Aikio et al.*, 2006]). The optical data from an all-sky camera, not shown, confirms that auroral activity spreads northward across the site at this time.

The T_i profiles (Figure 7c) show distinct structure during the time of the auroral activity, with increases in T_i corresponding to the gaps in N_e. These increases are consistent with large electric fields and horizontal flows

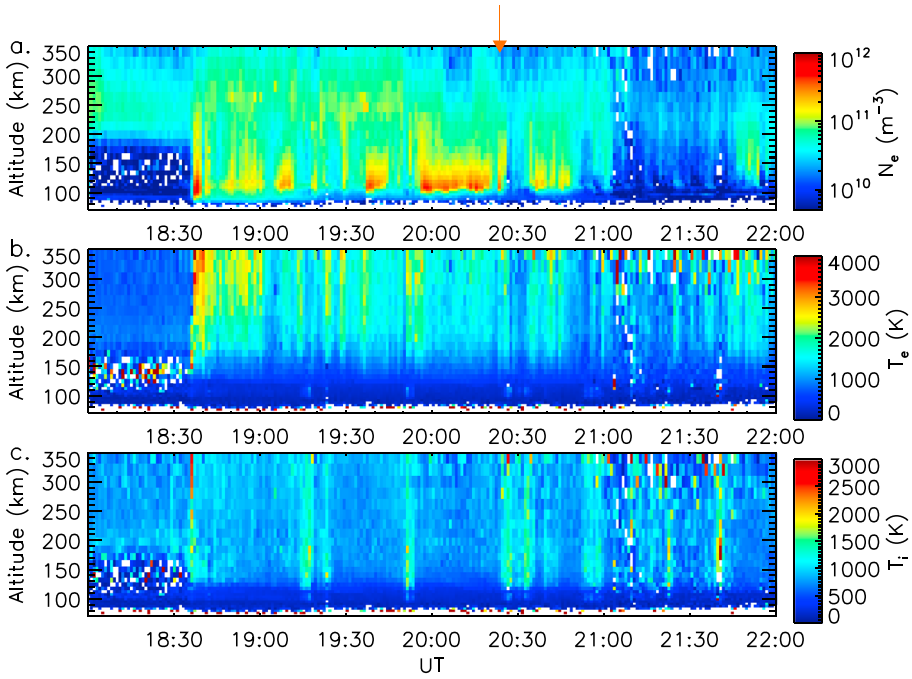

Figure 7. (a) Electron density, (b) electron temperature, and (c) ion temperature profiles between 17:00 and 22:00 UT from the ESR 42 m antenna at 60 s resolution. The orange arrow shows the time of analysis with ASK, ESR, and the respective models.

of ions in the region close to auroral brightness [*Lanchester et al.*, 1996]. This connection between a decrease in N_e and increase in T_i has also been reported and studied by *Opgenoorth et al.* [1990] and *Perry et al.* [2015].

The energy of the auroral precipitation can be estimated from the N_e profiles using the Southampton ionospheric model. The N_e profiles are converted to ionization rate profiles assuming a recombination rate coefficient, which is an assumption that affects the total flux estimate but does not affect the estimate of the energy of precipitation. The method, described in *Lanchester et al.* [1998], uses a library of both Gaussian and Maxwellian spectra to find the best fit for peak energy of precipitation. This analysis was applied to the same interval as was chosen in section 3.2.1 to estimate the precipitation energy using the ASK cameras between 20:23:25 and 20:24:00 UT, shown by an orange arrow above Figure 7a.

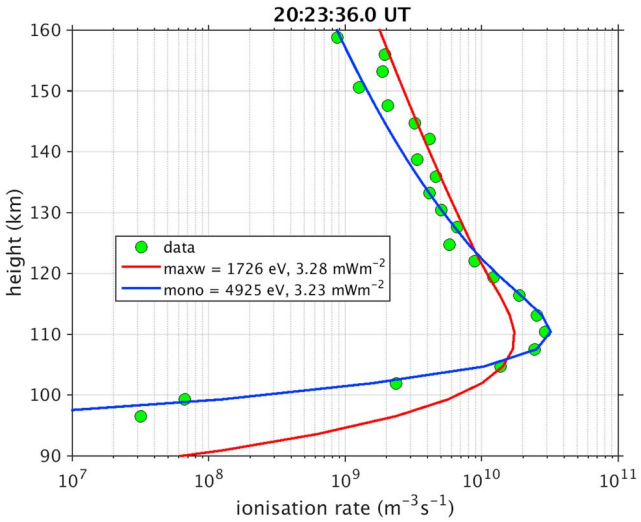

Figure 8. Ionization rate profile at 20:23:36 UT. Green dots are measurements at 2 s resolution. Blue line is the best fit to a monoenergetic/Gaussian input, red line is the best fit to a Maxwellian input.

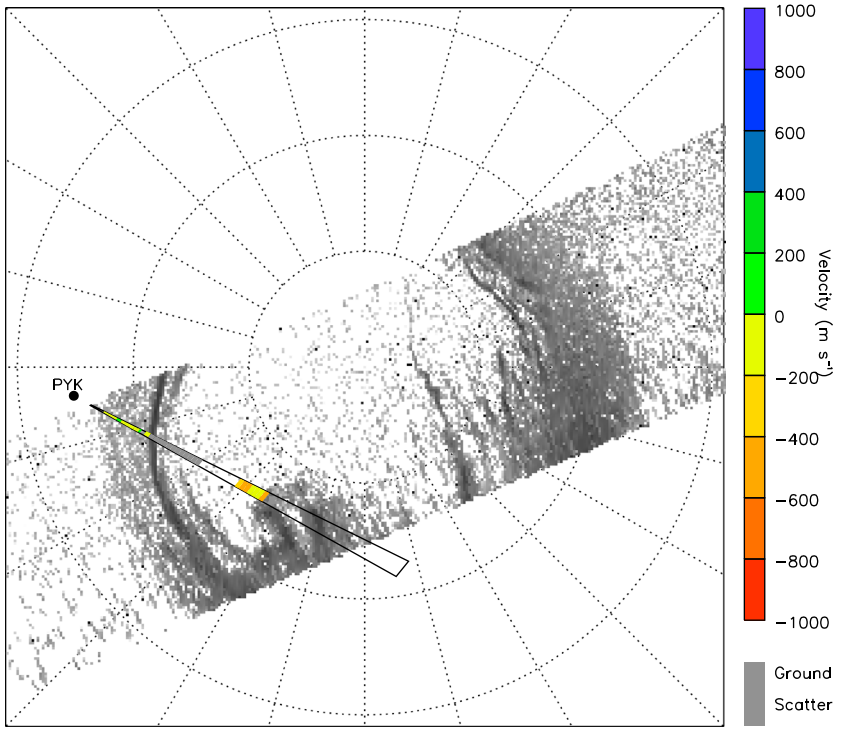

Figure 9. Velocity flows observed by the Pykkvibaer (PYK) radar from beam 5 at 18:58 UT. This radar is operating in stereo mode. Negative flows (red/orange) indicate flows away from the radar.

Figure 8 shows the results of this fitting process using an N_e profile at 20:23:36 UT. The data are shown in comparison with Maxwellian and monoenergetic (Gaussian) fits at 1.7 keV and 4.9 keV, respectively. This clearly shows that the data are a better fit to a Gaussian spectral shape. This result agrees with the analysis using the ASK emissions in Figure 6b, which has mean value of 5 keV. The combined ASK and ESR observations and associated modeling show that the energy of the precipitation is consistent with that typically seen on closed field lines.

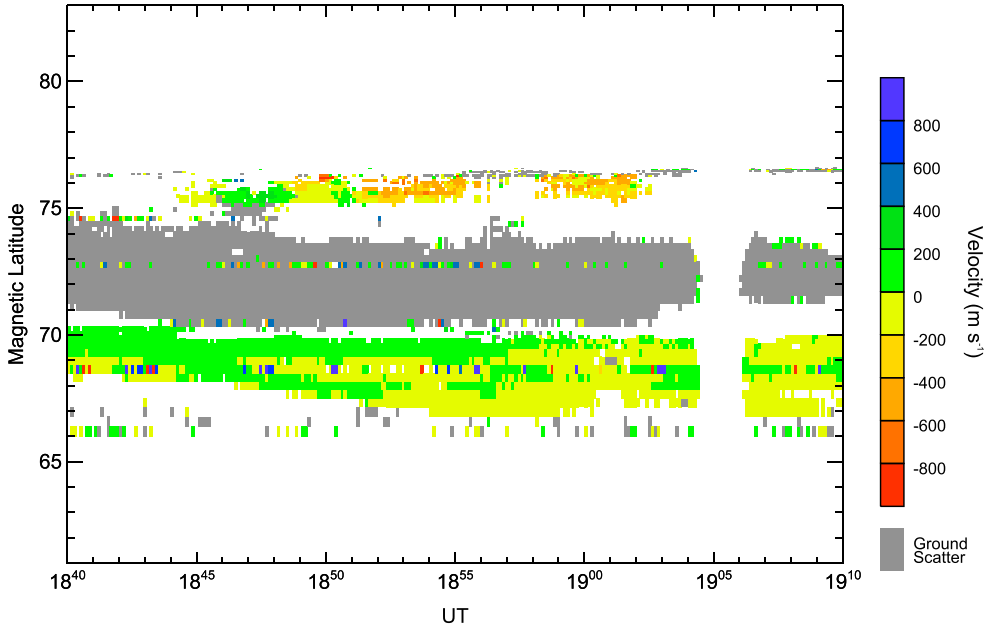

Figure 10. Time series between 18:40 and 19:10 UT of the velocity measurements obtained from PYK radar 5 in stereo mode [*Lester et al.*, 2004], again red/orange indicate flow away from the radar.

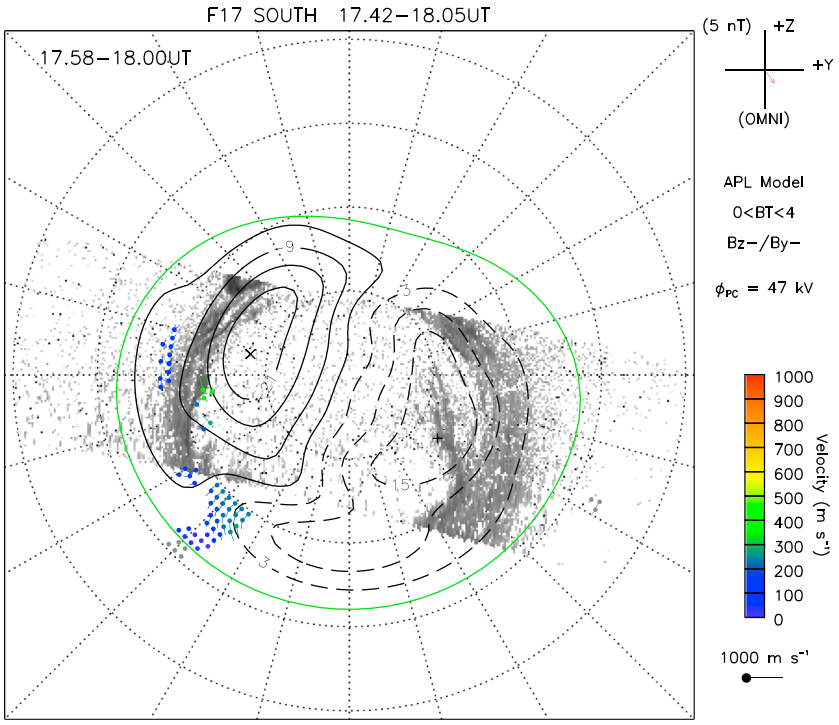

Figure 11. Map-potential plot of Southern Hemisphere SuperDARN data between 17:58 and 18:00 UT obtained using the method outline by *Ruohoniemi and Baker* [1998]. Data are plotted on top of the corresponding SSUSI image from DMSP F17 between 17:42 and 18:05 UT. Noon is at the top and dawn to the right.

3.2.3. SuperDARN Flows

The SuperDARN Pykkvibaer (PYK) radar has a field of view that covers the ASK and ESR sites and at the time of interest was operating in "stereo" mode [*Lester et al.*, 2004], in which two different experimental modes were operating simultaneously on different channels. The primary channel operated at 10.3 MHz in "common" mode, executing scans of the whole field of view, though no significant scatter was observed. The second channel (10.5 MHz) operated only on one beam (Beam 5) at higher temporal resolution. Figure 9 shows the spatial distribution of the data from one scan on this secondary channel at 18:58 UT in context with the Northern Hemisphere SSUSI image produced between 18:34 and 18:54 UT. Although these data appear spatially patchy (since data were only available from the one beam and the scatter is limited in extent along the beam) it can be seen in Figure 10, showing the time series of the line of sight velocity measurements observed by the radar between 18:40 and 19:10 UT, that these flows at 76° are persistent between 18:50 and 19:03 UT. Figure 9 illustrates that these flows coincide with the poleward edge of the bulge seen in the SSUSI image. A SuperDARN map-potential plot is not included here, as the only scatter in the area around the arc is provided by the PYK radar.

SuperDARN flows in the Southern Hemisphere were also examined. Figure 11 shows a map-potential plot at 17:42–18:05 UT in context with the Southern Hemisphere SSUSI image between 17:58 and 18:00 UT. The flow is spatially very localized between 20 and 22 MLT but shows apparent flow out of the polar cap approximately at the location the bulges form in the northern and southern polar caps. Figure 1c in *Fear and Milan* [2012b], shows a cartoon of nightside flow patterns of a transpolar arc whereby flux is closing in the tail and asymmetric flows are seen either side of the position of the transpolar arc. Hence, we suggest these flows are indicative of magnetotail reconnection under the influence of a B_y component, and hence consistent with the mechanism proposed by *Milan et al.* [2005] for transpolar arcs. Furthermore, although the data from the single radar beam shown in Figure 9 only tells us that there is ionospheric flow just duskward of the duskside feature that has a component directed away from the radar, we suggest that the localized but persistent flows seen at the tip of the duskside structure are at least consistent with the closure and exit of flux from the polar cap adjacent to the arc, and hence consistent with the transpolar arc mechanism.

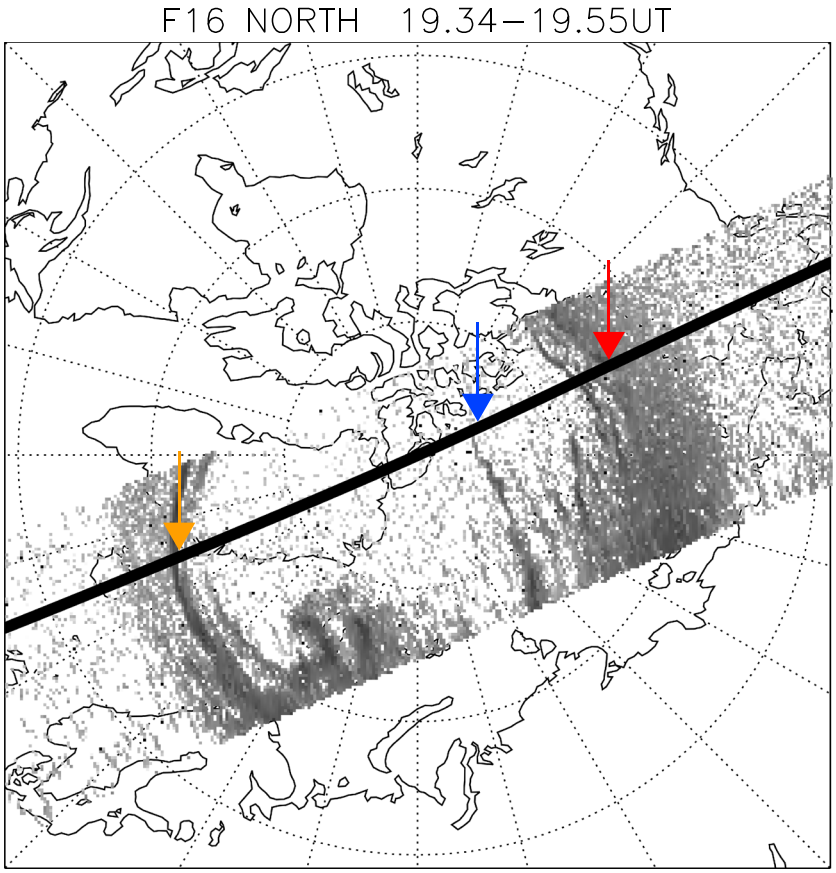

Figure 12. Footprint of the DMSP F16 spacecraft during the 19:34–19:55 UT pass, overplotted onto the corresponding SSUSI image. The arrows correspond to features in the DMSP particle spectrogram shown in Figure 13.

3.3. The Dawnside Sun-Aligned Arcs

3.3.1. DMSP

Figure 12 shows the footprint of the DMSP spacecraft during the 18:34–18:54 UT pass over the northern polar cap with corresponding SSUSI image. It can be seen that during this pass, DMSP intersected the tip of the farthest extended Sun-aligned arc on the dawnside of the polar cap but missed the structure on the duskside. The arrows correspond to the spacecraft crossing the duskward edge of the auroral oval (orange), the tip of the dawnside arc (blue), and the dawnside of the auroral oval (red). Figure 13a shows the spectra for each of these features in the corresponding colors. These spectra clearly show that the precipitation causing the dawnside arc is of lower energy than that above the auroral oval.

Figure 13b shows the DMSP electron spectrogram with the times of the three spectra indicated again with the orange, blue, and red arrows. The black vertical line marks the noon-midnight meridian, hence dividing the dawnside and duskside of the polar cap. Multiple low-energy features can be seen in the dawnside of the polar cap, the highest energy of these corresponds to the farthest protruding arc (blue arrow). Not all of these features can be seen in the corresponding SSUSI image (Figure 12), as they are too low in energy flux to be picked up by the UV imager. The ion spectrogram (Figure 13c) shows two ion signatures corresponding to each side of the auroral oval with no ion signatures within the polar cap between them. *Newell et al.* [2009] reported a common type of polar cap arc that can be identified by lower energy precipitation with no ion signature. They state this type of arc is consistent with accelerated polar rain, which *Carlson and Cowley* [2005] suggest can occur from shear flows on open field lines. Furthermore, the IMF conditions of negative B_x and positive B_y favor polar rain in the dawnside of the Northern Hemisphere polar cap [*Meng and Kroehl*, 1977; *Yeager and Frank*, 1975]. We hence suggest that the dawnside arc is an example of an arc formed by accelerated polar rain, occurring on open field lines.

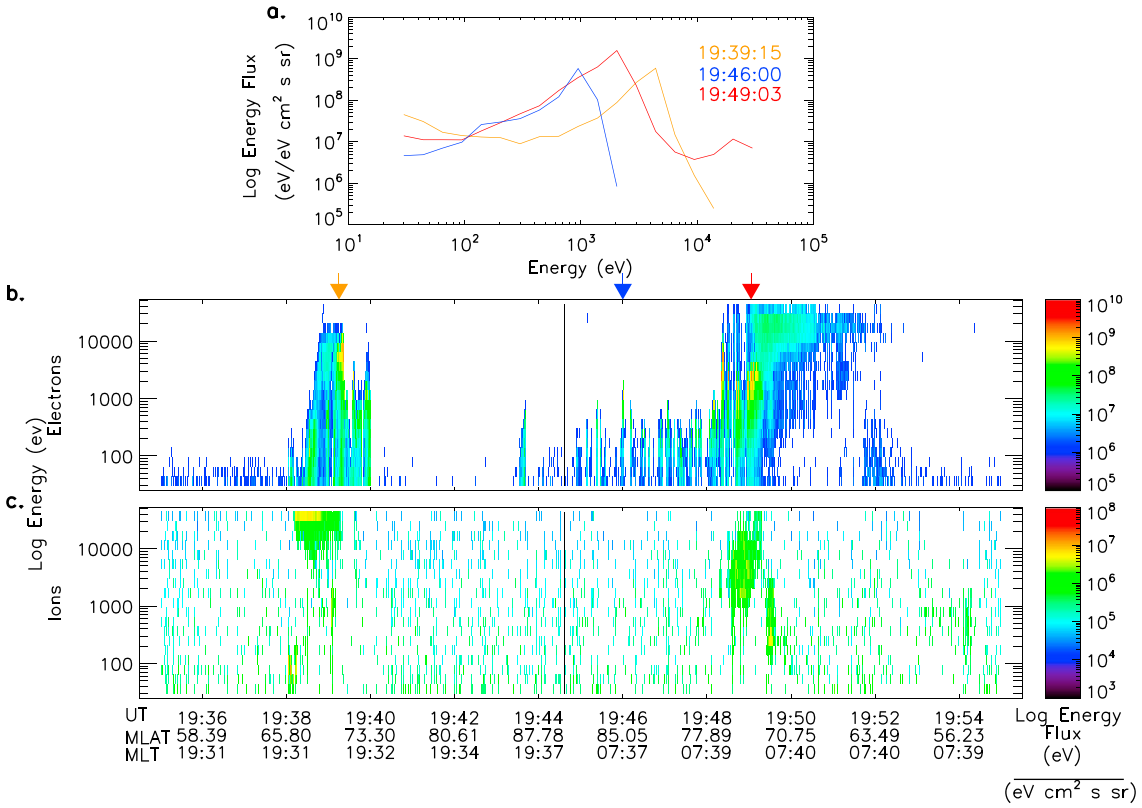

Figure 13. Data from the particle spectrograph SSJ4 onboard DMSP F16 between 19:34 and 19:55 UT. (a) Spectra (1 s) from the three times indicated by the arrows on the DMSP pass (Figure 12) at 19:39.15, 19:46.00, and 19:49.03 UT. (b) The electron spectrogram with the time of the above spectra indicated by the corresponding colored arrows. (c) The ion spectrogram. The black line seen in Figures 13b and 13c corresponds to the noon/midnight meridian to differentiate the dawnside and duskside of the polar cap.

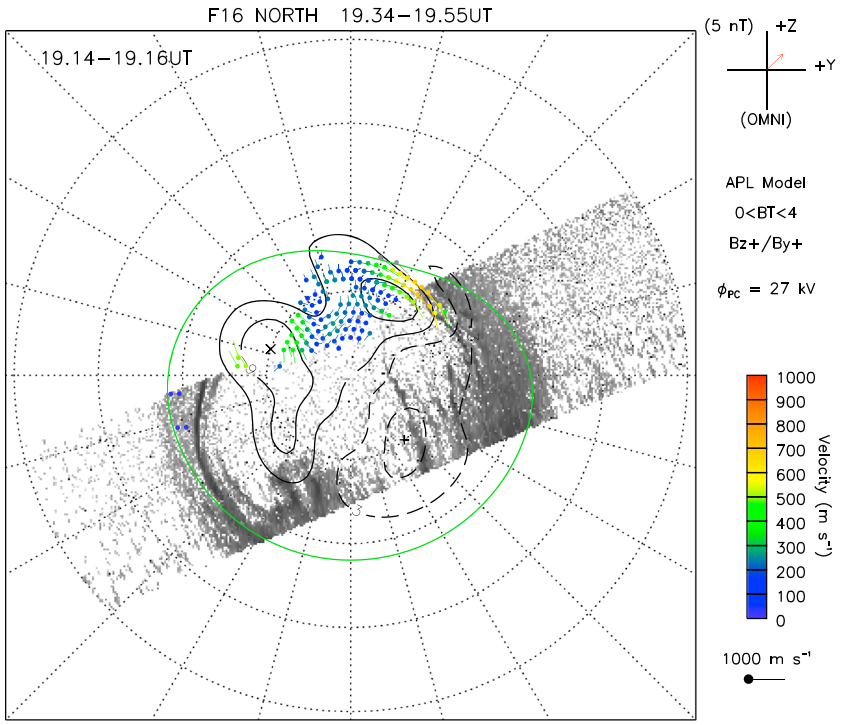

Figure 14. Map-potential plot of SuperDARN data between 19:14 and 19:16 UT with corresponding SSUSI image between 19:34 and 19:55 UT.

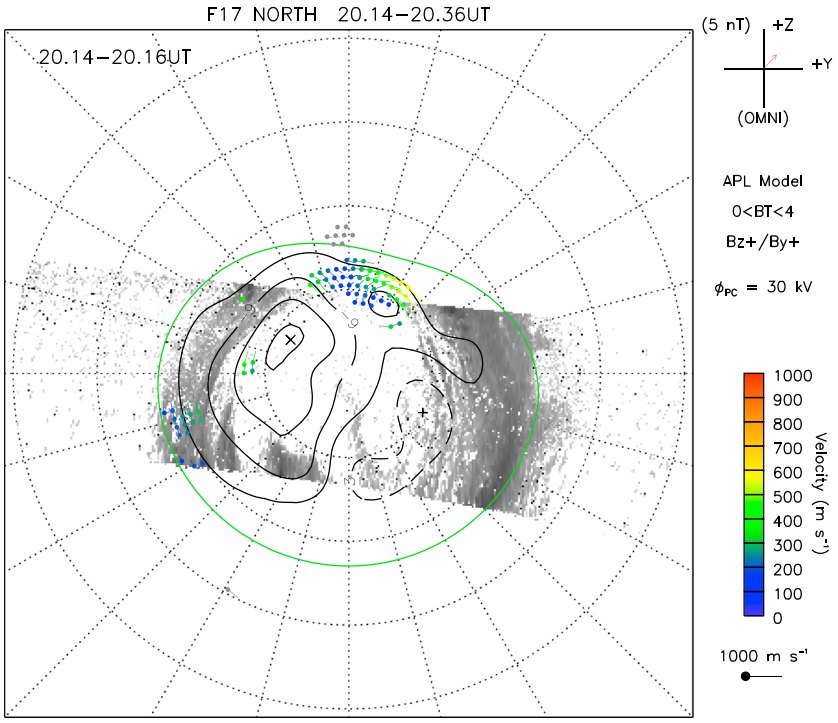

Figure 15. SuperDARN map-potential plot between 20:14 and 20:16 UT with corresponding SSUSI image between 20:14 and 20:36 UT.

As an additional point, Figures 13a and 13b show the oval electron signatures to have energy of the order of a few keV, with a peak on the duskside of 5 keV. These energies are very similar to those derived for the duskside structure from ASK and ESR and hence further supports the idea that this feature is formed on closed field lines.

3.3.2. SuperDARN Lobe Reconnection Flows

Examination of the map-potential plots from SuperDARN during our event revealed evidence of lobe reconnection between 19:12–19:30 UT and 20:10–21:00 UT. Examples are shown in Figures 14 and 15 at 19:14 UT and 20:14 UT, respectively, with the corresponding SSUSI image. Both images show sunward flows on the dayside of the polar cap and what appear to be dawnside lobe reconnection cells. The antisunward return flows appear to be poleward of the extension of the main oval from the SSUSI field of view, which is indicative of single-lobe reconnection [*Milan et al.*, 2000].

We previously noted that the farthest extended Sun-aligned arc on the dawnside moved duskward between SSUSI images seen in Figures 4a and 4c, which approximately corresponds to between 19:30 and 20:00 UT. This motion is consistent with what is expected observationally for positive IMF B_y [e.g., *Valladares et al.*, 1994]. It is also consistent with *Milan et al.* [2005] suggestion that the 'stirring' of flux caused by lobe reconnection in one hemisphere results in flux being transferred between dawn/dusk convection cells depending on the direction of IMF B_y. *Milan et al.* [2005] argued that this transferral of flux causes the arc, depending on its spatial location relative to the lobe convection, to move in the direction of IMF B_y, which is consistent with our observations.

4. Discussion

The structure seen by the SSUSI imager on the duskside of the Northern Hemisphere was analyzed with the ASK instrument and the ESR radar in conjunction with the Southampton ionospheric model to estimate the energy of the electron precipitation. This analysis revealed that the structure was associated with high-energy precipitation which likely occurred on closed field lines. The structure formed out of an auroral bulge. The small, localized disturbances in the Svalbard magnetometer data (Figure 3) coupled with the location of the bulge at the poleward edge of the oval suggested that it is formed by closure of flux at the far Earth neutral line, resulting in a poleward boundary intensification. This is further supported by SuperDARN

flows seen in Figure 11, which indicate that magnetotail reconnection was occurring around the position that the bulges formed in the polar cap. Flows measured by SuperDARN in the Northern Hemisphere (Figures 9 and 10) indicated that after the IMF turned northward, flux continued to close in the tail. Hence, we suggest, due to an assumed absence of low-latitude dayside reconnection from evidence of lobe reconnection (Figures 14 and 15), subsequently closed field lines protruded further into the polar cap instead of convecting back to the dayside. Furthermore, the map-potential plot in Figure 11 shows flows exiting the polar cap at 21 MLT which indicate that the IMF B_y component is having an effect on reconnection in the tail. These observations are consistent with the mechanism described in *Milan et al.* [2005] for transpolar arcs. However, as the structure does not cross the entire polar cap, we conclude that it is an example of a "failed" transpolar arc. The transpolar arc most likely failed due to a cessation in nightside reconnection between 19:30 and 20:30 UT when the structure was seen to stay at the same magnetic latitude in the SSUSI images (i.e., between Figures 2c and 4a). This claim is somewhat supported by the fact that we see no evidence of nightside reconnection in the SuperDARN data (such as those seen earlier in Figures 9 and 11) during this interval (not shown). Furthermore, the structure is no longer seen by SSUSI after 20:40 UT (also not shown), which coincides with the Southward turning of the IMF (Figure 1).

The *Milan et al.* [2005] mechanism predicts that the transpolar arc would form on the duskside of the northern polar cap for positive IMF B_y, statistically verified by *Fear and Milan* [2012a], which is consistent with the conditions for this event. However, the Southern Hemisphere counterpart also appears on the duskside, which is not consistent with the *Milan et al.* [2005] mechanism. *Grocott* [2016] suggests that there are two factors which lead to asymmetric flows seen in the polar cap, as seen in the Southern Hemisphere SuperDARN observations (Figure 11). The first factor is a twist in the magnetotail occurring after a few hours of B_y influence and results in asymmetries between auroral onset location in the Northern and Southern Hemispheres, which is why the *Milan et al.* [2005] mechanism predicts transpolar arcs on opposite sides of the polar cap in the different hemispheres. The second factor is caused by dawn-dusk asymmetries in the plasma sheet occurring after longer periods of stable B_y, which results in a shift in the auroral onset location to earlier MLT for positive B_y and later for negative B_y. A study by *Reistad et al.* [2016] reported a 3 h MLT shift in the auroral morphology seen by simultaneous measurements from the IMAGE FUV-WIC camera in the Northern Hemisphere and the Polar VIS Earth camera in the Southern Hemisphere. This shift was seen on the duskside of the auroral oval and was attributed to a persistent positive IMF B_y component, which led to asymmetries in the magnetospheric footprints. The second mechanism suggested by *Grocott* [2016] appears to be consistent with our event since the IMF B_y component in the hours before the period of interest (Figure 1) and in the previous 24 h (not shown) was predominately positive and the structures appear on the same side of the polar cap. Hence, our event could be evidence for the two factors being present at the same time, an idea speculated by *Grocott* [2016] or could suggest that the lack of dayside reconnection rather than the twist in the magnetotail is the key factor in the *Milan et al.* [2005] mechanism for this case.

The multiple, Sun-aligned arcs seen in the dawnside Northern Hemisphere polar cap appear to be formed by a different mechanism than the duskside structure. They were only seen in one hemisphere of the SSUSI images (Figures 2 and 4) and the DMSP particle data showed the farthest protruding arc to be of lower energy than the oval and duskside structure and not associated with an ion signature (Figure 13). This is different from the DMSP observations of a transpolar arc in a study by *Fear et al.* [2014], which showed the arc to be associated with high-energy electron (up to 10 keV) and ion (greater than 1 keV) signatures. They also saw lower energy electron-only signatures, which did not have a counterpart in IMAGE and suggested that these may be associated with fainter polar cap arcs that form on open field lines. These features are more consistent with the DMSP precipitation associated with the dawnside arcs in this study. *Fear et al.* [2014] also presented observation from Cluster that showed that the plasma source for this arc was on closed field lines. Similarly, a study by *Mailyan et al.* [2015] presented observations of a transpolar arc (observed by IMAGE and the TIMED/GUVI instrument, which is very similar to SSUSI) and a conjugate in situ plasma signature detected by Cluster. The electron and ion signatures observed by Cluster were at lower energies than those observed by *Fear et al.* [2014]. *Mailyan et al.* [2015] were unable to determine whether the plasma and auroral signature observed were on open or closed magnetic field lines, but did identify fainter arcs in the GUVI image that branched away from the main transpolar arc. They also presented DMSP particle data with electron-only signatures of comparable energy to our event, which are suggested to be associated with these fainter arcs. They suggest that these fainter arcs are formed on open field lines associated with solar wind direct entry, advocated by *Shi et al.* [2013] to be due to high-latitude magnetopause reconnection. One problem with this interpretation

is that the high-latitude magnetopause reconnection site maps to the cusp spot, which is just poleward of the auroral oval on the dayside [*Sandholt et al.*, 1996, 1998; *Øieroset et al.*, 1997], rather than farther tailward where the arcs are observed. Our suggested mechanism (acceleration of polar rain) is subtly different, as the plasma is free to enter across the full width of the lobe (which is open), in a manner controlled by the IMF B_x/B_y components [*Meng and Kroehl*, 1977; *Yeager and Frank*, 1975], but the acceleration is localized to the field lines which map to the arcs.

Newell et al. [2009] suggest polar cap arcs that do not have an ion signature and are not adjacent to the auroral oval could be produced by enhanced polar rain. It can be seen in Figure 13b that the Sun-aligned arc on the dawnside of the Northern Hemisphere polar cap is embedded within similar features of lower energy, which are not seen in the SSUSI image. These features are similar to what *Shinohara and Kokubun* [1996] classify as type B polar showers, i.e., polar showers without ion fluxes that respond to solar wind conditions (appearing on the dawnside for positive B_y and Northern Hemisphere for negative B_x) and hence suggested to originate from the solar wind. Therefore, we conclude that these Sun-aligned arcs are consistent with accelerated polar rain and hence formed on open field lines.

We have shown that the dawnside arcs move duskward with the flow in the lobe convection cells. This duskward motion for positive IMF B_y is consistent with previous studies which observed polar cap arcs to move in the same direction as IMF B_y. *Milan et al.* [2005] suggest that the convection caused by the stirring of the lobes will cause polar cap arcs in the Northern Hemisphere to convect duskward/dawnward for IMF B_y positive/negative, respectively. This pattern is observed during our event. As an additional point, the duskside structure was seen by the SIF ground-based camera to move from west to east, i.e., dawnward (see movies in the supporting information). This motion also fits with the *Milan et al.* [2005] mechanism, but the arc moves oppositely to the direction of IMF B_y because it is on the other side of the polar cap and hence moving with the dusk cell. However, this structure would have been classified by *Hosokawa et al.* [2011] as a "B_y independent" as it is moving poleward irrespective of the direction of IMF B_y. Hence, "B_y-dependent" and "B_y-independent" arcs can both be explained by the *Milan et al.* [2005] mechanism.

5. Conclusion

A case study of polar cap aurora occurring on 19 January 2008 has been presented. Almost simultaneous observations of the northern and southern auroral regions were provided by the SSUSI instruments on board DMSP F16 and F17. Two different types of high-latitude aurora were observed simultaneously in the northern polar cap; a "failed" transpolar arc on the duskside formed on closed field lines, and Sun-aligned arc on the dawnside, which was more consistent with precipitation on open field lines.

The duskside structure had a conjugate form in the Southern Hemisphere, which also formed on the duskside on the southern polar cap. The structure started as a bulge, identified in magnetometer data as a poleward boundary intensification, which grew into a distinctly Sun-aligned structure. The Northern Hemisphere structure was examined using ground-based instruments. Using observations from the ASK instrument in conjunction with the Southampton ionospheric model, the electron precipitation energy above the dusk structure was estimated to be between 2 and 11 keV and confirmed by fitting electron density profiles from the ESR to be monoenergetic in spectral shape. It was shown that these energies are similar to the measurements made by the DMSP particle spectrometer of the auroral oval. Images from the ASK1 camera also revealed highly structured and dynamic small-scale filamentary aurora. It was concluded that the duskside structure was consistent with aurora formed on closed field lines. ESR electron temperature profiles showed very cold plasma prior to the onset of the aurora on closed field lines, hence suggesting that these closed field lines were within the open field lines of the polar cap. Coupled with the signatures of nightside reconnection observed in the SuperDARN data, we find this duskside structure to be consistent with the mechanism proposed by *Milan et al.* [2005] for transpolar arcs. However, in this case the structure did not cross the entire polar cap and hence we suggest it is an example of a "failed" transpolar arc. The arc perhaps failed due to a sudden cessation of nightside reconnection. Furthermore, the fact that this feature was shown to form from a poleward boundary intensification is consistent with the idea that transpolar arcs (failed or otherwise) are formed from magnetotail reconnection.

The second type of structure was only seen in the Northern Hemisphere SSUSI images and was analyzed using data from the DMSP particle spectrometer. This Sun-aligned arc was associated with lower energy electrons than in the oval and no ion signature. It also appeared on the dawnside of the Northern Hemisphere polar cap,

which is consistent with statistics for polar rain. Hence, this arc is suggested to be an example of the common weaker polar cap arcs described in *Newell et al.* [2009], consistent with acceleration of polar rain on open field lines.

Evidence has been presented for two processes occurring simultaneously in the polar cap during northward IMF resulting in the formation of different polar cap auroral features. This work shows that the magnetosphere can have a configuration which allows multiple processes for the formation of polar cap arcs to occur simultaneously, during northward IMF. Further study is needed to explore the open field line mechanism resulting in the lower energy high-latitude aurora and also what causes the cessation of nightside reconnection, which ultimately lead the transpolar arc to fail.

Acknowledgments
This work was supported by the Natural Environmental Research Council (NERC) studentship NE/L002531/1. R.C.F was supported by the United Kingdom's Science and Technology Facilities Council (STFC) Ernest Rutherford FellowshipST/K004298/2. D.K.W and B.S.L are supported by NERC grant NE/N004051/1. M.L. is supported by NERC grant NE/K011766/1. Cluster data were obtained from the Cluster Science Archive http://www.cosmos.esa.int/web/csa/access. The DMSP particle detectors were designed by D. Hardy of Air Force Research Laboratory, and data were obtained from the Johns Hopkins University Applied Physics Laboratory. The IMAGE magnetometer data are collected as a joint European collaboration. FMI serves as the PI-institute in the collaboration. Svalbard magnetometer data are provided by the University of Tromso. EISCAT is an international association supported by research organizations in China (CRIRP), Finland (SA), Japan (NIPR and STEL), Norway (NFR), Sweden (VR), and the United Kingdom (NERC). ASK has been funded by PPARC, NERC, and STFC of the United Kingdom and the Swedish Research Council. For the data used in the research, we thank the EISCAT and ASK campaign teams for running the instruments during several winter campaigns. Requests for data used in this paper can be directed to Jade Reidy (jr10g11@soton.ac.uk) or http://ask1.esr.eiscat.no/contact.html. The authors acknowledge the use of SuperDARN data. SuperDARN is a collection of radars funded by national scientific funding agencies of Australia, Canada, China, France, Japan, South Africa, United Kingdom, and the United States of America. Data were obtained from the British Antarctic Survey SuperDARN data hub, and we are grateful to Paul Breen for his assistance. We thank Adrian Grocott, Jonny Rae, Clare Watt and Noora Partamies for useful discussions during this study.

References

Aikio, A. T., T. Pitkänen, A. Kozlovsky, and O. Amm (2006), Method to locate the polar cap boundary in the nightside ionosphere and application to a substorm event, *Ann. Geophys.*, *24*, 1905–1917, doi:10.5194/angeo-24-1905-2006.

Ashrafi, M. (2007), ASK: Auroral Structure and Kinetics in action, *Astron. Geophys.*, *48*(4), 4.35–4.37, doi:10.1111/j.1468-4004.2007.48435.x.

Balogh, A., et al. (2001), The Cluster magnetic field investigation: Overview of in-flight performance and initial results, *Ann. Geophys.*, *19*, 1207–1217, doi:10.5194/angeo-19-1207-2001.

Berkey, F. T., L. L. Cogger, S. Ismail, and Y. Kamide (1976), Evidence for a correlation between Sun-aligned arcs and the interplanetary magnetic field direction, *Geophys. Res. Lett.*, *3*, 145–147, doi:10.1029/GL003i003p00145.

Browett, S. D., R. C. Fear, A. Grocott, and S. E. Milan (2016), Timescales for the penetration of IMF B_Y into the Earth's magnetotail, *J. Geophys. Res. Space Physics*, *122*, 579–593, doi:10.1002/2016JA023198.

Carlson, H. C., and S. W. H. Cowley (2005), Accelerated polar rain electrons as the source of Sun-aligned arcs in the polar cap during northward interplanetary magnetic field conditions, *J. Geophys. Res*, *110*, A05302, doi:10.1029/2004JA010669.

Carter, J. A., S. E. Milan, R. C. Fear, A. Kullen, and M. R. Hairston (2015), Dayside reconnection under interplanetary magnetic field B_y-dominated conditions: The formation and movement of bending arcs, *J. Geophys. Res*, *120*, 2967–2978, doi:10.1002/2014JA020809.

Chisham, G., et al. (2007), A decade of the Super Dual Auroral Radar Network (SuperDARN): Scientific achievements, new techniques and future directions, *Surv. Geophys.*, *28*, 33–109, doi:10.1007/s10712-007-9017-8.

Craven, J. D., J. S. Murphree, L. L. Cogger, and L. A. Frank (1991), Simultaneous optical observations of transpolar arcs in the two polar caps, *Geophys. Res. Lett.*, *18*, 2297–2300, doi:10.1029/91GL02308.

Crooker, N. U., and F. J. Rich (1993), Lobe cell convection as a summer phenomenon, *J. Geophys. Res.*, *98*, 13403–13407, doi:10.1029/93JA01037.

Dahlgren, H., N. Ivchenko, J. Sullivan, B. S. Lanchester, G. Marklund, and D. Whiter (2008), Morphology and dynamics of aurora at fine scale: First results from the ASK instrument, *Ann. Geophys.*, *26*, 1041–1048, doi:10.5194/angeo-26-1041-2008.

Dahlgren, H., A. Aikio, K. Kaila, N. Ivchenko, B. Lanchester, D. Whiter, and G. Marklund (2010), Simultaneous observations of small multi-scale structures in an auroral arc, *J. Atmos. Sol. Terr. Phys.*, *72*(7), 633–637.

Dahlgren, H., B. Gustavsson, B. S. Lanchester, N. Ivchenko, U. Brändström, D. K. Whiter, T. Sergienko, I. Sandahl, and G. Marklund (2011), Energy and flux variations across thin auroral arcs, *Ann. Geophys.*, *29*, 1699–1712, doi:10.5194/angeo-29-1699-2011.

Dahlgren, H., B. S. Lanchester, N. Ivchenko, and D. K. Whiter (2016), Electrodynamics and energy characteristics of aurora at high resolution by optical methods, *J. Geophys. Res. Space Physics*, *121*, 5966–5974, doi:10.1002/2016JA022446.

Dandouras, I., A. Barthe, E. Penou, S. Brunato, H. Rème, L. M. Kistler, M. B. Bavassano-Cattaneo, and A. Blagau (2010), Cluster Ion Spectrometry (CIS) data in the Cluster Active Archive (CAA), in *The Cluster Active Archive, Studying the Earth's Space Plasma Environment*, vol. 11, edited by H. Laakso, M. G. T. T. Taylor, and C. P. Escoubet, pp. 51–72, Springer, Berlin, doi:10.1007/978-90-481-3499-1_3.

Davis, T. N. (1963), Negative correlation between polar-cap visual aurora and magnetic activity, *J. Geophys. Res.*, *68*, 4447–4453.

Eriksson, S., et al. (2005), On the generation of enhanced sunward convection and transpolar aurora in the high-latitude ionosphere by magnetic merging, *J. Geophys. Res.*, *110*, A11218, doi:10.1029/2005JA011149.

Fear, R. C., and S. E. Milan (2012a), The IMF dependence of the local time of transpolar arcs: Implications for formation mechanism, *J. Geophys. Res*, *117*, A03213, doi:10.1029/2011JA017209.

Fear, R. C., and S. E. Milan (2012b), Ionospheric flows relating to transpolar arc formation, *J. Geophys. Res*, *117*, A09230, doi:10.1029/2012JA017830.

Fear, R. C., S. E. Milan, R. Maggiolo, A. N. Fazakerley, I. Dandouras, and S. B. Mende (2014), Direct observation of closed magnetic flux trapped in the high-latitude magnetosphere, *Science*, *346*, 1506–1510, doi:10.1126/science.1257377.

Fear, R. C., S. E. Milan, J. A. Carter, and R. Maggiolo (2015), The interaction between transpolar arcs and cusp spots, *Geophys. Res. Lett.*, *42*, 9685–9693, doi:10.1002/2015GL066194.

Frank, L. A., J. D. Craven, J. L. Burch, and J. D. Winningham (1982), Polar views of the Earth's aurora with Dynamics Explorer, *Geophys. Res. Lett.*, *9*, 1001–1004, doi:10.1029/GL009i009p01001.

Frank, L. A., J. D. Craven, and R. L. Rairden (1985), Images of the Earth's aurora and geocorona from the Dynamics Explorer mission, *Adv. Space Res.*, *5*, 53–68, doi:10.1016/0273-1177(85)90116-4.

Frank, L. A., J. D. Craven, D. A. Gurnett, S. D. Shawhan, J. L. Burch, J. D. Winningham, C. R. Chappell, J. H. Waite, N. C. Maynard, and M. Sugiura (1986), The theta aurora, *J. Geophys. Res*, *91*, 3177–3224, doi:10.1029/JA091iA03p03177.

Gloag, J. M., E. A. Lucek, L.-N. Alconcel, A. Balogh, P. Brown, C. M. Carr, C. N. Dunford, T. Oddy, and J. Soucek (2010), FGM data products in the CAA, in *The Cluster Active Archive, Studying the Earth's Space Plasma Environment*, vol. 11, edited by H. Laakso, M. G. T. T. Taylor, and C. P. Escoubet, pp. 109–128, Springer, Berlin, doi:10.1007/978-90-481-3499-1_7.

Goudarzi, A., M. Lester, S. E. Milan, and H. U. Frey (2008), Multi-instrumentation observations of a transpolar arc in the Northern Hemisphere, *Ann. Geophys.*, *26*, 201–210, doi:10.5194/angeo-26-201-2008.

Greenwald, R. A., et al. (1995), Darn/Superdarn: A global view of the dynamics of high-lattitude convection, *Space Sci. Rev.*, *71*, 761–796, doi:10.1007/BF00751350.

Grocott, A. (2016), Dawn-dusk asymmetries in planetary plasma environment, in *Time-dependence of dawn-dusk asymmetries in the terrestrial ionospheric convection pattern*, p. 341, AGU, Washington, D. C.

Grocott, A., S. W. H. Cowley, and J. B. Sigwarth (2003), Ionospheric flow during extended intervals of northward but B_y-dominated IMF, *Ann. Geophys.*, *21*, 509–538, doi:10.5194/angeo-21-509-2003.

Grocott, A., T. K. Yeoman, S. E. Milan, O. Amm, H. U. Frey, L. Juusola, R. Nakamura, C. J. Owen, H. Rème, and T. Takada (2007), Multi-scale observations of magnetotail flux transport during IMF-northward non-substorm intervals, *Ann. Geophys.*, *25*, 1709–1720, doi:10.5194/angeo-25-1709-2007.

Gussenhoven, M. S. (1982), Extremely high latitude auroras, *J. Geophys. Res*, *87*, 2401–2412, doi:10.1029/JA087iA04p02401.

Hardy, D. A., W. J. Burke, and M. S. Gussenhoven (1982), DMSP optical and electron measurements in the vicinity of polar cap arcs, *J. Geophys. Res*, *87*, 2413–2430, doi:10.1029/JA087iA04p02413.

Hedin, A. E. (1991), Extension of the MSIS thermosphere model into the middle and lower atmosphere, *J. Geophys. Res.*, *96*, 1159–1172, doi:10.1029/90JA02125.

Hoffman, R. A., R. A. Heelis, and J. S. Prasad (1985), A Sun-aligned arc observed by DMSP and AE-C, *J. Geophys. Res*, *90*, 9697–9710, doi:10.1029/JA090iA10p09697.

Hosokawa, K., J. I. Moen, K. Shiokawa, and Y. Otsuka (2011), Motion of polar cap arcs, *J. Geophys. Res*, *116*, A01305, doi:10.1029/2010JA015906.

Huang, C. Y., J. D. Craven, and L. A. Frank (1989), Simultaneous observations of a theta aurora and associated magnetotail plasmas, *J. Geophys. Res.*, *94*, 10,137–10,143, doi:10.1029/JA094iA08p10137.

Kullen, A., M. Brittnacher, J. A. Cumnock, and L. G. Blomberg (2002), Solar wind dependence of the occurrence and motion of polar auroral arcs: A statistical study, *J. Geophys. Res*, *107*, 1362, doi:10.1029/2002JA009245.

Kullen, A., R. C. Fear, S. E. Milan, J. A. Carter, and T. Karlsson (2015), The statistical difference between bending arcs and regular polar arcs, *J. Geophys. Res. Space Physics*, *120*, 10,443–10,465, doi:10.1002/2015JA021298.

Lanchester, B. S., K. Kailá, and I. W. McCrea (1996), Relationship between large horizontal electric fields and auroral arc elements, *J. Geophys. Res.*, *101*, 5075–5084, doi:10.1029/95JA02055.

Lanchester, B. S., M. H. Rees, K. J. F. Sedgemore, J. R. Palmer, H. U. Frey, and K. U. Kaila (1998), Ionospheric response to variable electric fields in small-scale auroral structures, *Ann. Geophys.*, *16*, 1343–1354, doi:10.1007/s00585-998-1343-8.

Lanchester, B. S., M. H. Rees, D. Lummerzheim, A. Otto, K. J. F. Sedgemore-Schulthess, H. Zhu, and I. W. McCrea (2001), Ohmic heating as evidence for strong field-aligned currents in filamentary aurora, *J. Geophys. Res*, *106*, 1785–1794, doi:10.1029/1999JA000292.

Lanchester, B. S., M. Ashrafi, and N. Ivchenko (2009), Simultaneous imaging of aurora on small scale in OI (777.4 nm) and $N_2$1P to estimate energy and flux of precipitation, *Ann. Geophys.*, *27*, 2881–2891, doi:10.5194/angeo-27-2881-2009.

Lavraud, B., M. F. Thomsen, M. G. G. T. Taylor, Y. L. Wang, T. D. Phan, S. J. Schwartz, R. C. Elphic, A. Fazakerley, H. RèMe, and A. Balogh (2005), Characteristics of the magnetosheath electron boundary layer under northward interplanetary magnetic field: Implications for high-latitude reconnection, *J. Geophys. Res.*, *110*, A06209, doi:10.1029/2004JA010808.

Lester, M., et al. (2004), Stereo CUTLASS—A new capability for the SuperDARN HF radars, *Ann. Geophys.*, *22*, 459–473, doi:10.5194/angeo-22-459-2004.

Lühr, H., A. Aylward, S. C. Bucher, A. Pajunpää, K. Pajunpää, T. Holmboe, and S. M. Zalewski (1998), Westward moving dynamic substorm features observed with the IMAGE magnetometer network and other ground-based instruments, *Ann. Geophys.*, *16*, 425–440, doi:10.1007/s00585-998-0425-y.

Lummerzheim, D. (1987), Electron transport and optical emissions in the aurora, PhD thesis, Alaska Univ., Fairbanks.

Lyons, L. R., T. Nagai, G. T. Blanchard, J. C. Samson, T. Yamamoto, T. Mukai, A. Nishida, and S. Kokobun (1999), Association between Geotail plasma flows and auroral poleward boundary intensifications observed by CANOPUS photometers, *J. Geophys. Res*, *104*, 4485–4500, doi:10.1029/1998JA900140.

Mailyan, B., et al. (2015), Transpolar arc observation after solar wind entry into the high-latitude magnetosphere, *J. Geophys. Res. Space Physics*, *120*, 3525–3534, doi:10.1002/2014JA020912.

Mawson, D. (1916), Auroral observations at the Cape Royds station, Antarctica, *Trans. Proc. R. Soc. S. Aust.*, *60*, 151–212.

Meng, C.-I. (1981), Polar cap arcs and the plasma sheet, *Geophys. Res. Lett.*, *8*, 273–276, doi:10.1029/GL008i003p00273.

Meng, C.-I., and H. W. Kroehl (1977), Intense uniform precipitation of low-energy electrons over the polar cap, *J. Geophys. Res*, *82*, 2305–2313, doi:10.1029/JA082i016p02305.

Milan, S. E., M. Lester, S. W. H. Cowley, and M. Brittnacher (2000), Dayside convection and auroral morphology during an interval of northward interplanetary magnetic field, *Ann. Geophys.*, *18*, 436–444, doi:10.1007/s00585-000-0436-9.

Milan, S. E., B. Hubert, and A. Grocott (2005), Formation and motion of a transpolar arc in response to dayside and nightside reconnection, *J. Geophys. Res*, *110*, A01212, doi:10.1029/2004JA010835.

Newell, P. T., K. Liou, and G. R. Wilson (2009), Polar cap particle precipitation and aurora: Review and commentary, *J. Atmos. Sol. Terr. Phys.*, *71*, 199–215, doi:10.1016/j.jastp.2008.11.004.

Øieroset, M., P. E. Sandholt, W. F. Denig, and S. W. H. Cowley (1997), Northward interplanetary magnetic field cusp aurora and high-latitude magnetopause reconnection, *J. Geophy. Res.*, *102*, 11,349–11,362, doi:10.1029/97JA00559.

Opgenoorth, H. J., I. Haggstrom, P. J. S. Williams, and G. O. L. Jones (1990), Regions of strongly enhanced perpendicular electric fields adjacent to auroral arcs, *J. Atmos. Sol. Terr. Phys.*, *52*, 449–458, doi:10.1016/0021-9169(90)90044-N.

Østgaard, N., S. B. Mende, H. U. Frey, L. A. Frank, and J. B. Sigwarth (2003), Observations of non-conjugate theta aurora, *Geophys. Res. Lett.*, *30*, 2125, doi:10.1029/2003GL017914.

Paxton, L. J., D. Morrison, Y. Zhang, H. Kil, B. Wolven, B. S. Ogorzalek, D. C. Humm, and C.-I. Meng (2002), Validation of remote sensing products produced by the Special Sensor Ultraviolet Scanning Imager (SSUSI): A far UV-imaging spectrograph on DMSP F-16, in *Optical Spectroscopic Techniques, Remote Sensing, and Instrumentation for Atmospheric and Space Research IV*, vol. 4485, edited by A. M. Larar and M. G. Mlynczak, pp. 338–348, doi:10.1117/12.454268.

Perry, G. W., H. Dahlgren, M. J. Nicolls, M. Zettergren, J.-P. St.-Maurice, J. L. Semeter, T. Sundberg, K. Hosokawa, K. Shiokawa, and S. Chen (2015), Spatiotemporally resolved electrodynamic properties of a Sun-aligned arc over Resolute Bay, *J. Geophys. Res. Space Physics*, *120*, 9977–9987, doi:10.1002/2015JA021790.

Reistad, J. P., N. Østgaard, P. Tenfjord, K. M. Laundal, K. Snekvik, S. Haaland, S. E. Milan, K. Oksavik, H. U. Frey, and A. Grocott (2016), Dynamic effects of restoring footpoint symmetry on closed magnetic field lines, *J. Geophys. Res. Space Physics*, *121*, 3963–3977, doi:10.1002/2015JA022058.

Rème, H., et al. (2001), First multispacecraft ion measurements in and near the Earth's magnetosphere with the identical Cluster Ion Spectrometry (CIS) experiment, *Ann. Geophys.*, *19*, 1303–1354, doi:10.5194/angeo-19-1303-2001.

Ruohoniemi, J. M., and K. B. Baker (1998), Large-scale imaging of high-latitude convection with Super Dual Auroral Radar Network HF radar observations, *J. Geophys. Res.*, *103*, 20,797–20,811, doi:10.1029/98JA01288.

Sandholt, P. E., C. J. Farrugia, M. Øieroset, P. Stauning, and S. W. H. Cowley (1996), Auroral signature of lobe reconnection, *J. Geophys. Res.*, *23*, 1725–1728, doi:10.1029/96GL01846.

Sandholt, P. E., C. J. Farrugia, J. Moen, and S. W. H. Cowley (1998), Dayside auroral configurations: Responses to southward and northward rotations of the interplanetary magnetic field, *J. Geophys. Res.*, *103*, 20,279–20,296, doi:10.1029/98JA01541.

Shi, Q. Q., et al. (2013), Solar wind entry into the high-latitude terrestrial magnetosphere during geomagnetically quiet times, *Nat. Commun.*, *4*, 1466, doi:10.1038/ncomms2476.

Shinohara, I., and S. Kokubun (1996), Statistical properties of particle precipitation in the polar cap during intervals of northward interplanetary magnetic field, *J. Geophys. Res*, *101*, 69–82, doi:10.1029/95JA01848.

Tanskanen, E. I. (2009), A comprehensive high-throughput analysis of substorms observed by IMAGE magnetometer network: Years 1993–2003 examined, *J. Geophys. Res*, *114*, A05204, doi:10.1029/2008JA013682.

Tenfjord, P., N. Østgaard, K. Snekvik, K. M. Laundal, J. P. Reistad, S. Haaland, and S. E. Milan (2015), How the IMF B_y induces a B_y component in the closed magnetosphere and how it leads to asymmetric currents and convection patterns in the two hemispheres, *J. Geophys. Res. Space Physics*, *120*, 9368–9384, doi:10.1002/2015JA021579.

Valladares, C. E., H. C. Carlson Jr., and K. Fukui (1994), Interplanetary magnetic field dependency of stable Sun-aligned polar cap arcs, *J. Geophys. Res.*, *99*, 6247–6272, doi:10.1029/93JA03255.

Wannberg, G., et al. (1997), The EISCAT Svalbard radar: A case study in modern incoherent scatter radar system design, *Radio Sci.*, *32*, 2283–2307, doi:10.1029/97RS01803.

Whiter, D. K., B. S. Lanchester, B. Gustavsson, N. Ivchenko, and H. Dahlgren (2010), Using multispectral optical observations to identify the acceleration mechanism responsible for flickering aurora, *J. Geophys. Res*, *115*, A12315, doi:10.1029/2010JA015805.

Wu, Q., T. J. Rosenberg, F. T. Berkey, and R. H. Eather (1991), Intensification and fading of auroral arcs in the dusk-midnight sector of the polar cap, *J. Geophys. Res*, *96*, 7709–7719, doi:10.1029/91JA00256.

Yeager, D. M., and L. A. Frank (1975), Low-energy electron intensities at large distances over the Earth's polar cap, *J. Geophys. Res.*, *81*, 3966–3976.

Zhu, L., R. W. Schunk, and J. J. Sojka (1997), Polar cap arcs: A review, *J. Atmos. Sol. Terr. Phys.*, *59*, 1087–1126, doi:10.1016/S1364-6826(96)00113-7.